Robotica (2022), **40**, pp. 1257–1273
doi:10.1017/S0263574721000953

CAMBRIDGE
UNIVERSITY PRESS

RESEARCH ARTICLE

Optimal motion control of three-sphere based low-Reynolds number swimming microrobot

Hossein Nejat Pishkenari* and Matin Mohebalhojeh

Nano-Robotics Laboratory, Mechanical Engineering Department, Sharif University of Technology, Tehran, Iran
*Corresponding author. E-mail: nejat@sharif.edu

Received: 24 October 2020; **Revised:** 19 June 2021; **Accepted:** 22 June 2021; **First published online:** 2 September 2021

Keywords: Microrobot; Swimmer; Low-Reynolds number; Dynamic Modeling; Optimal Control

Abstract

Microrobots with their promising applications are attracting a lot of attention currently. A microrobot with a triangular mechanism was previously proposed by scientists to overcome the motion limitations in a low-Reynolds number flow; however, the control of this swimmer for performing desired manoeuvres has not been studied yet. Here, we have proposed some strategies for controlling its position. Considering the constraints on arm lengths, we proposed an optimal controller based on quadratic programming. The simulation results demonstrate that the proposed optimal controller can steer the microrobot along the desired trajectory as well as minimize fluctuations of the actuators length.

Nomenclature

a	Sphere radius (μm)
U_{ij}	Distance between centers of sphere i and sphere j, $i, j = 1,\ 2,\ 3.$ (μm)
μ	Fluid viscosity ($kg.m^{-1}.s^{-1}$)
$\mathbf{v}$	Fluid velocity ($m.\ s^{-1}$)
p	Fluid pressure (Pa)
$\mathbf{f}_j$, $\mathbf{v}_i$	Force acting on sphere i (N), velocity of sphere i ($m.\ s^{-1}$)
$\mathbf{H}_{ij}$	Hydrodynamic Oseen tensor ($m.\ s^{-1}.N^{-1}$)
$\mathbf{r}_i$, $\mathbf{r}_{ij}$	Position vector of sphere center i (μm), position vector of sphere center i relative to sphere center j (μm)
$\mathbf{I}$	Identity matrix (-)
x_i, y_i, z_i	x, y, and z positions of sphere i in three-dimensional Cartesian coordinate system (μm)
θ	Angle between arm connecting spheres 1 and 2 and x axis (radians)
$(x_1)_d$, $(y_1)_d$	Desired x and y positions of sphere 1 (μm)
$(\theta)_d$	Desired θ (radians)
k_{p1}, k_{p2}, k_{p3}	Proportional control coefficients (s^{-1})
Δt	Simulation time step (s)
J	Optimization objective function
L	Lagrange function

1. Introduction

New advances in science and technology have opened the fields of microrobotics and microsystems for research. As a result, microrobots have become of great importance, with a variety of applications

in different fields [1]. Some of the most important and significant of these applications can be found in the field of medicine, where microrobots can help in advancing modern and revolutionary medical techniques [2]. Inspired from nature, different mechanisms have been proposed for microrobots [3].

Microrobots play an important role in efforts toward developing targeted drug delivery methods. The small scale of microrobotic swimmers enables them to carry and deliver doses of high concentration drug in a small target region, minimalizing the side effects on other organs [4,5]. In addition, small scale means that microrobots can potentially be used for various noninvasive surgical procedures and material removal within the body [3]. Microsystems can also be used for probing regions of the body for assessing patients' health and searching for tumors within the body [6]. Artificial fertilization using microrobots has also been proposed. In this case, swimming microrobots are usually used for carrying sperm cells and driving them inside the egg cell for insemination [7].

Much work has been conducted on the underlying physics of swimming microorganisms and the modeling of their motion [8]. The physics governing micro swimmer motion is the same for artificial and biological swimmers, and many microrobotic designs are drawn from inspirations from nature. Therefore, methods developed for modeling biological microswimmers can also be used for modeling the motion of artificial microswimmers. Furthermore, designs for the swimming mechanisms of microrobots can be based on biological swimming mechanisms in microorganisms, and artificial microswimmers are usually inspired by natural swimmers [9,10]. Similarly, materials and methods have been proposed to imitate biological swimming mechanisms in artificial microswimmers [11].

Bacteria are among the most common microorganisms that have inspired models for microrobots. Based on their motion, helical microrobots have been proposed and analyzed which use a rotating helical flagellum as a means of propulsion [12,13]. The models based on bacterium motion have also been expanded to consider the motion of microswimmers consisting of two or more flagella [14,15]. A mechanism has also been proposed that consists of two parallel flagella rotating around one axis [16]. In this mechanism, the rotation of the outer flagellum mainly produces propulsion, while the inner flagellum is responsible for controlling forward velocity.

In addition, models based on microorganisms other than bacteria, such as ciliates, have been proposed [17,18]. Difficulties in fabricating structures at microscale have also led some researchers to propose micro-bio-robots, which are propelled using microorganisms [19,20]. All of the aforementioned models require an understanding of the basics of swimming motion at microscale where the Reynolds number is small. Purcell [21] showed that microswimmer motion creates low-Reynolds number flow, which can be described using the linear, time-independent Stokes equation. He demonstrated that microswimmers cannot move using a reciprocal mechanism and must employ nonreciprocal means of applying force on the fluid. (This behavior is known as the scallop theorem [21].) Based on this theorem, several microswimmers have been proposed during recent years [22–26]. To name but a few, Rizvi et al. [24] introduced a triangular three-bead microswimmer where three identical springs connect the beads. A triangular mechanism for planar motion has been proposed by Ebrahimian et al. [25]. Khalesi et al. [26] have proposed an innovative magnetic microswimmer. Esfandbod et al. [27] introduced a three-dimensional microswimmer capable of high maneuverability.

Although a significant progress has been made in the design and dynamic modeling of microswimmers, development of control strategies for such microrobots has not been addressed in a satisfactory manner. Here, we aim to design some control strategies for the microswimmer proposed by Ebrahimian et al. [25], which can be extended to other similar microswimmers too. The microswimmer proposed by Ebrahimian et al. has been referred to as the low-Reynolds number predator and consists of three spheres of radius $a = 1\ \mu\text{m}$, attached together by three arms in a triangular formation. This mechanism is illustrated in Fig. 1. Ebrahimian et al. have also proposed a cycle of strokes, which results in translational and rotational motion.

The dynamics of these models have been fully analyzed and simulated using the linear equations governing low-Reynolds number flows. However, in most cases, controlling the motion of these swimmers

https://doi.org/10.1017/S0263574721000953 Published online by Cambridge University Press

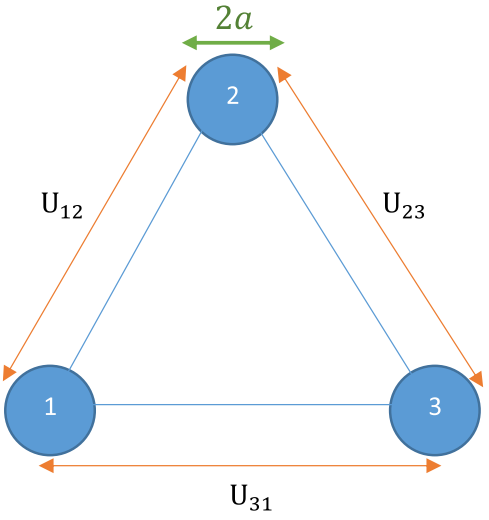

Figure 1. *Triangular microswimmer proposed by Ebrahimian et al. [25].*

has not been considered by the researchers that have proposed these models, because the motivation for coming up with these models and analyzing them has usually been to analyze and simulate the motion of biological microswimmers and better understand their movement.

In this paper, we have used the triangular model proposed by Ebrahimian et al. as a model for a swimming microrobot which is tasked with successfully tracking down a desired path. In doing so, we have also bridged a gap in research by proposing a number of strategies for controlling the motion of this swimmer. The proposed control schemes are a simple nonoptimal controller, an optimal controller without considering constraints on the robot arm length, an optimal controller considering the constraints on arm lengths. The control parameters are the swimmer's arm lengths, and the objective of the control strategies is to ensure that microrobot is able to track its desired path. In this case, the microrobot and the ideal path can also be viewed in a predator-prey paradigm, where the predator (microrobot) needs to track down and hunt its prey (ideal path). Efficiency and minimization of energy consumption and path tracking with arm length constraints have been key factors in proposing novel techniques for optimal control of the predator's position.

This paper has been organized in the following order: first, in Section 2, the dynamical equations of the predator have been obtained. Next, at the end of Section 2, the dynamical motion of the predator has been simulated according to the strokes proposed in [25]. After the results of dynamical simulation have been verified with [25], the motion of the swimming predator has been controlled under various control strategies. First, in Section 3, the motion of one sphere and orientation angle of one arm has been controlled to follow the desired path of a prey. Then, in Section 4, optimal control and path tracking of one sphere has been analyzed. After that, in Section 5, optimal control of one sphere along with arm length constraints has been discussed. Ultimately, results and simulations from various control strategies have been discussed and compared.

2. Governing Equations

The small scale of microswimmers results in a low-Reynolds flow regime. As a result, the Navier–Stokes equations reduce to the linear, time-independent Stokes equation. Therefore, fluid flow resulting from a swimming microrobot is governed by the Stokes and continuity equations [23]. For an incompressible

https://doi.org/10.1017/S0263574721000953 Published online by Cambridge University Press

Newtonian fluid, the equations are as follows [28]:

$$\nabla \cdot \mathbf{v} = 0, \qquad -\nabla \mathrm{p} + \mu \nabla^2 \mathbf{v} = 0, \tag{1}$$

where $\mathbf{v}$ denotes the fluid velocity vector, p is the fluid pressure, and μ is the fluid viscosity. In modeling the microrobot, dynamic interactions between the arms and the fluid are neglected, mainly because of their relative slenderness. Therefore, Eq. (1) need to be solved subject to no-slip conditions relative to the spheres and $\mathbf{v} = 0$ at infinity. It is also assumed that forces acting on each sphere pass through its center.

The relation between each sphere's velocity and the forces acting on each sphere can be presented as follows [25]:

$$\mathbf{v}_i = \sum_{j=1}^{3} \mathbf{H}_{ij} \mathbf{f}_j, \tag{2}$$

where $\mathbf{v}_i$ is the velocity of sphere i, $\mathbf{f}_j$ is the force acting on sphere j, and $\mathbf{H}_{ij}$ is the symmetric Oseen tensor, which depends on the geometry of the system. For a system of linked spherical swimmers, $\boldsymbol{H}_{ij}$ can be written as follows [29]:

$$\mathbf{H}_{ij} = \begin{cases} \frac{1}{6\pi\mu a}\mathbf{I}, & \text{if } i = j \\ \frac{1}{8\pi\mu|\mathbf{r}_{ij}|}\left(\mathbf{I} + \frac{\mathbf{r}_{ij}\mathbf{r}_{ij}}{|\mathbf{r}_{ij}|^2}\right), & \text{if } i \neq j \end{cases} \tag{3}$$

where $\mathbf{r}_{ij} = \mathbf{r}_i - \mathbf{r}_j$, and $\mathbf{r}_i$ is the position vector of sphere i. Here $\mathbf{I}$ is the identity matrix of size 3. Along with Eq. (3), the microswimmer's motion is also subject to the conservation of linear and angular momentum [25]:

$$\sum_{i=1}^{3} \mathbf{f}_i = 0, \qquad \sum_{i=1}^{3} \mathbf{r}_i \times \mathbf{f}_i = 0. \tag{4}$$

The set of equations in (2) and (4) forms the dynamic equations of the swimming predator.

2.1 Derivation of Oseen tensor

In order to use Eq. (2), we derive the explicit form of the hydrodynamic Oseen tensor presented in relation (3). The center of each sphere is presented in a three-dimensional Cartesian coordinate system, where x_i, y_i, and z_i represent the coordinates of sphere i. The relative distances are shown in the following order:

$$z_{ij} = z_i - z_j, \quad y_{ij} = y_i - y_j, \quad x_{ij} = x_i - x_j, \tag{5}$$

$$\mathbf{r}_{ij} = \mathbf{r}_i - \mathbf{r}_j = \begin{bmatrix} x_{ij} \\ y_{ij} \\ z_{ij} \end{bmatrix}, \qquad |\mathbf{r}_{ij}| = \sqrt{{x_{ij}}^2 + {y_{ij}}^2 + {z_{ij}}^2}. \tag{6}$$

Accordingly, for $i \neq j$, $\mathbf{H}_{ij}$ can be obtained in the following order:

$$\mathbf{H}_{ij} = \frac{1}{8\pi\mu\,|\mathbf{r}_{ij}|}\left(\mathbf{I} + \frac{\mathbf{r}_{ij}\mathbf{r}_{ij}}{|\mathbf{r}_{ij}|^2}\right) = \frac{1}{8\pi\mu\,|\mathbf{r}_{ij}|}\left(\begin{bmatrix} 1 & 0 & 0 \\ 0 & 1 & 0 \\ 0 & 0 & 1 \end{bmatrix} + \frac{\begin{bmatrix} {x_{ij}}^2 & x_{ij}y_{ij} & x_{ij}z_{ij} \\ y_{ij}x_{ij} & {y_{ij}}^2 & y_{ij}z_{ij} \\ z_{ij}x_{ij} & z_{ij}y_{ij} & {z_{ij}}^2 \end{bmatrix}}{{x_{ij}}^2 + {y_{ij}}^2 + {z_{ij}}^2}\right) \tag{7}$$

https://doi.org/10.1017/S0263574721000953 Published online by Cambridge University Press

In the case where $i = j$:

$$\mathbf{H}_{ij} = \frac{1}{6\pi\mu a}\mathbf{I} = \frac{1}{6\pi\mu a}\begin{bmatrix} 1 & 0 & 0 \\ 0 & 1 & 0 \\ 0 & 0 & 1 \end{bmatrix}. \tag{8}$$

In the case where a microswimmer's motion is two-dimensional, Eqs. (7) and (8) can be simplified for two-dimensional motion:

$$\mathbf{H}_{ii} = \frac{1}{6\pi\mu a}\begin{bmatrix} 1 & 0 \\ 0 & 1 \end{bmatrix}, \qquad \mathbf{H}_{ij} = \frac{\begin{bmatrix} 2x_{ij}^{\,2} + y_{ij}^{\,2} & x_{ij}y_{ij} \\ y_{ij}x_{ij} & x_{ij}^{\,2} + 2y_{ij}^{\,2} \end{bmatrix}}{8\pi\mu\left(x_{ij}^{\,2} + y_{ij}^{\,2}\right)^{\frac{3}{2}}} \tag{9}$$

Eq. (9) yields the Oseen tensor for a two-dimensional, three-sphere microsystem.

2.2 Derivation of the Governing Equations of Motion

The explicit form of the low-Reynolds predator's equations of motion can be obtained by expanding Eqs. (2) and (4) in terms of the hydrodynamic Oseen tensor in (9). First, Eq. (2) needs to be expanded. To this end, distances between spheres i and j are represented by U_{ij}, and forces exerted on sphere i are shown by $\begin{pmatrix} \mathrm{f}_{xi} \\ \mathrm{f}_{yi} \end{pmatrix}$. The position of each sphere center is represented according to Eqs. (5) and (6).

Merging Eqs. (2) and (9) results in the following matrix equation:

$$\dot{\mathbf{x}} = \mathbf{G}\mathbf{f}. \tag{10}$$

Here, $\dot{\mathbf{x}} = [\dot{x}_1 \quad \dot{y}_1 \quad \dot{x}_2 \quad \dot{y}_2 \quad \dot{x}_3 \quad \dot{y}_3]^{\mathrm{T}}$ and $\mathbf{f} = [\mathrm{f}_{x1} \quad \mathrm{f}_{y1} \quad \mathrm{f}_{x2} \quad \mathrm{f}_{y2} \quad \mathrm{f}_{x3} \quad \mathrm{f}_{y3}]^{\mathrm{T}}$. $\mathbf{G}$ is a 6×6 matrix which depends on the relative position of each sphere's center:

$$\mathbf{G} = \begin{bmatrix} \frac{1}{6\pi\mu a} & 0 & \frac{2x_{12}^{\,2}+y_{12}^{\,2}}{8\pi\mu \mathrm{U}_{12}^{\,3}} & \frac{x_{12}y_{12}}{8\pi\mu \mathrm{U}_{12}^{\,3}} & \frac{2x_{13}^{\,2}+y_{13}^{\,2}}{8\pi\mu \mathrm{U}_{31}^{\,3}} & \frac{x_{13}y_{13}}{8\pi\mu \mathrm{U}_{31}^{\,3}} \\ 0 & \frac{1}{6\pi\mu a} & \frac{y_{12}x_{12}}{8\pi\mu \mathrm{U}_{12}^{\,3}} & \frac{x_{12}^{\,2}+2y_{12}^{\,2}}{8\pi\mu \mathrm{U}_{12}^{\,3}} & \frac{y_{13}x_{13}}{8\pi\mu \mathrm{U}_{31}^{\,3}} & \frac{x_{13}^{\,2}+2y_{13}^{\,2}}{8\pi\mu \mathrm{U}_{31}^{\,3}} \\ \frac{2x_{12}^{\,2}+y_{12}^{\,2}}{8\pi\mu \mathrm{U}_{12}^{\,3}} & \frac{x_{12}y_{12}}{8\pi\mu \mathrm{U}_{12}^{\,3}} & \frac{1}{6\pi\mu a} & 0 & \frac{2x_{23}^{\,2}+y_{23}^{\,2}}{8\pi\mu \mathrm{U}_{23}^{\,3}} & \frac{x_{23}y_{23}}{8\pi\mu \mathrm{U}_{23}^{\,3}} \\ \frac{y_{12}x_{12}}{8\pi\mu \mathrm{U}_{12}^{\,3}} & \frac{x_{12}^{\,2}+2y_{12}^{\,2}}{8\pi\mu \mathrm{U}_{12}^{\,3}} & 0 & \frac{1}{6\pi\mu a} & \frac{y_{23}x_{23}}{8\pi\mu \mathrm{U}_{23}^{\,3}} & \frac{x_{23}^{\,2}+2y_{23}^{\,2}}{8\pi\mu \mathrm{U}_{23}^{\,3}} \\ \frac{2x_{13}^{\,2}+y_{13}^{\,2}}{8\pi\mu \mathrm{U}_{31}^{\,3}} & \frac{x_{13}y_{13}}{8\pi\mu \mathrm{U}_{31}^{\,3}} & \frac{2x_{23}^{\,2}+y_{23}^{\,2}}{8\pi\mu \mathrm{U}_{23}^{\,3}} & \frac{x_{23}y_{23}}{8\pi\mu \mathrm{U}_{23}^{\,3}} & \frac{1}{6\pi\mu a} & 0 \\ \frac{y_{13}x_{13}}{8\pi\mu \mathrm{U}_{31}^{\,3}} & \frac{x_{13}^{\,2}+2y_{13}^{\,2}}{8\pi\mu \mathrm{U}_{31}^{\,3}} & \frac{y_{23}x_{23}}{8\pi\mu \mathrm{U}_{23}^{\,3}} & \frac{x_{23}^{\,2}+2y_{23}^{\,2}}{8\pi\mu \mathrm{U}_{23}^{\,3}} & 0 & \frac{1}{6\pi\mu a} \end{bmatrix}. \tag{11}$$

Eq. (10) can alternatively be written as

$$\mathbf{f} = \mathbf{G}^{-1}\dot{\mathbf{x}}. \tag{12}$$

The motion of this microswimmer is controlled by changing the length of each arm using prismatic actuators. Therefore, we are interested in writing the force vector in terms of a combination of velocity and time derivatives of the length of each arm. This can be achieved by deriving the relation between the following two sets of variables:

$$\dot{\mathbf{x}} = \mathbf{D}\dot{\mathbf{z}}, \tag{13}$$

where $\dot{\mathbf{z}} = \begin{bmatrix} \dot{x}_1 & \dot{y}_1 & \dot{\theta}_{12} & \dot{\mathrm{U}}_{12} & \dot{\mathrm{U}}_{23} & \dot{\mathrm{U}}_{31} \end{bmatrix}^{\mathrm{T}}$. Matrix $\mathbf{D}$ in relation (13) can be determined by obtaining time derivatives of geometric relations presented in Fig. 2. Using relationship between spheres

https://doi.org/10.1017/S0263574721000953 Published online by Cambridge University Press

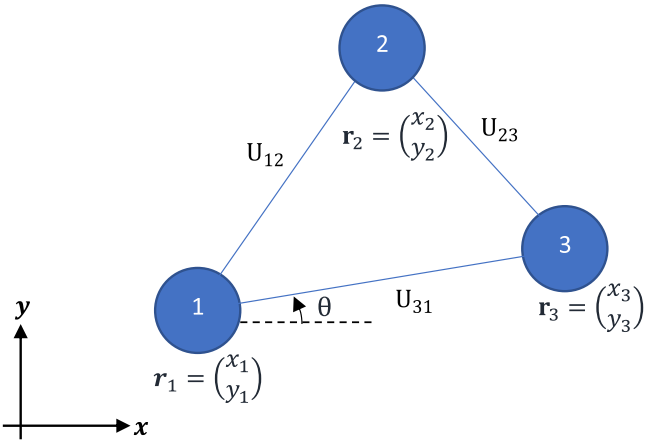

Figure 2. *Position vector of each sphere center in x-y coordinate and angle* θ.

coordinates and after some mathematical manipulation, we can obtain:

$$\dot{\mathbf{x}} = \begin{bmatrix} \dot{x}_1 \\ \dot{y}_1 \\ \dot{x}_2 \\ \dot{y}_2 \\ \dot{x}_3 \\ \dot{y}_3 \end{bmatrix} = \begin{bmatrix} 1 & 0 & 0 & 0 & 0 & 0 \\ 0 & 1 & 0 & 0 & 0 & 0 \\ E_{11} & E_{12} & E_{13} & E_{14} & E_{15} & E_{16} \\ E_{21} & E_{22} & E_{23} & E_{24} & E_{25} & E_{26} \\ 1 & 0 & -y_{31} & 0 & 0 & \frac{x_{31}}{U_{31}} \\ 0 & 1 & x_{31} & 0 & 0 & \frac{y_{31}}{U_{31}} \end{bmatrix} \begin{bmatrix} \dot{x}_1 \\ \dot{y}_1 \\ \dot{\theta} \\ \dot{U}_{12} \\ \dot{U}_{23} \\ \dot{U}_{31} \end{bmatrix} = \mathbf{D}\dot{\mathbf{z}}, \tag{14}$$

where $\mathbf{E} = \mathbf{A}^{-1}\mathbf{B}\mathbf{C}$, $\mathbf{A} = \begin{bmatrix} x_{12} & y_{12} \\ x_{23} & y_{23} \end{bmatrix}$, $\mathbf{B} = \begin{bmatrix} x_{12} & y_{12} & 0 & 0 & -U_{12} & 0 \\ 0 & 0 & x_{23} & y_{23} & 0 & U_{23} \end{bmatrix}$, and $\mathbf{C} = \begin{bmatrix} 1 & 0 & 0 & 0 & 0 & 0 \\ 0 & 1 & 0 & 0 & 0 & 0 \\ 1 & 0 & -y_{31} & 0 & 0 & \frac{x_{31}}{U_{31}} \\ 0 & 1 & x_{31} & 0 & 0 & \frac{y_{31}}{U_{31}} \\ 0 & 0 & 0 & 1 & 0 & 0 \\ 0 & 0 & 0 & 0 & 1 & 0 \end{bmatrix}$. Here E_{ij} are the elements of matrix **E**. Hence, Eq. (12) can be written in the following form:

$$\mathbf{f} = \mathbf{G}^{-1}\dot{\mathbf{x}} = \mathbf{M}\dot{\mathbf{z}}, \tag{15}$$

where $\mathbf{M} = \mathbf{G}^{-1}\mathbf{D}$. Now using Eqs. (4) and (15) we can obtain:

$$[\mathbf{M}_1 \quad \mathbf{M}_2 \quad \mathbf{M}_3]^{\mathrm{T}}[\dot{x}_1 \quad \dot{y}_1 \quad \dot{\theta} \quad \dot{U}_{12} \quad \dot{U}_{23} \quad \dot{U}_{31}]^{\mathrm{T}} = 0, \tag{16}$$

where $\mathbf{M}_1 = \begin{bmatrix} 1 & 0 & 1 & 0 & 1 & 0 \end{bmatrix}\mathbf{M}$, $\mathbf{M}_2 = \begin{bmatrix} 0 & 1 & 0 & 1 & 0 & 1 \end{bmatrix}\mathbf{M}$, and $\mathbf{M}_3 = \begin{bmatrix} -y_1 & x_1 & -y_2 & x_2 & -y_3 & x_3 \end{bmatrix}\mathbf{M}$. Relation (16), which consists of three equations and six variables, describes the dynamic properties of the microrobot. It can be used alongside Eq. (13) to determine the position of each sphere's center.

2.3 Dynamic simulation and validation

If at each point in time, the length of each arm is known, Eq. (16) yields a system of three equations and three variables, which can be solved in each time step. Here, we have simulated an ordered motion consisting of six steps and two cycles. In the first cycle, each arm shrinks from L to $L^* = (1 - \epsilon)$ L, with

https://doi.org/10.1017/S0263574721000953 Published online by Cambridge University Press

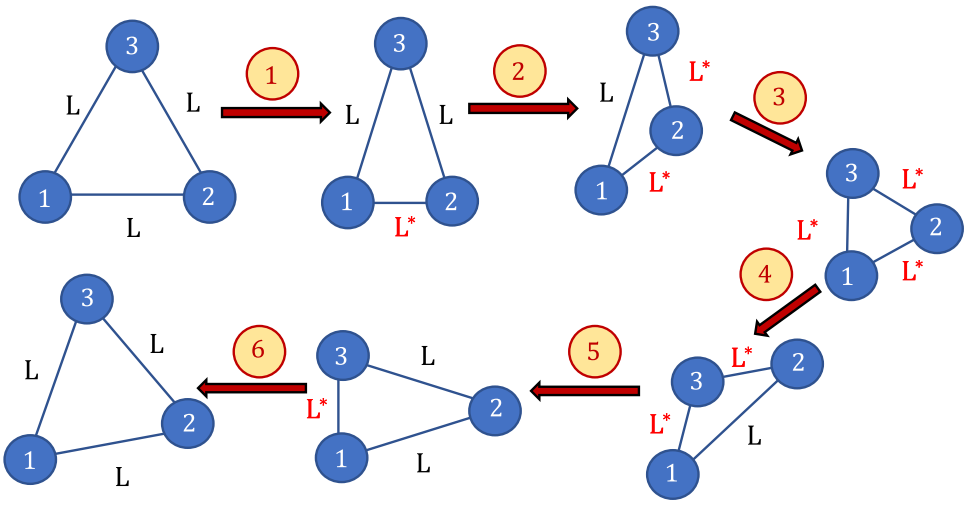

Figure 3. *The order by which each arm shrinks and then returns to its original configuration [25].*

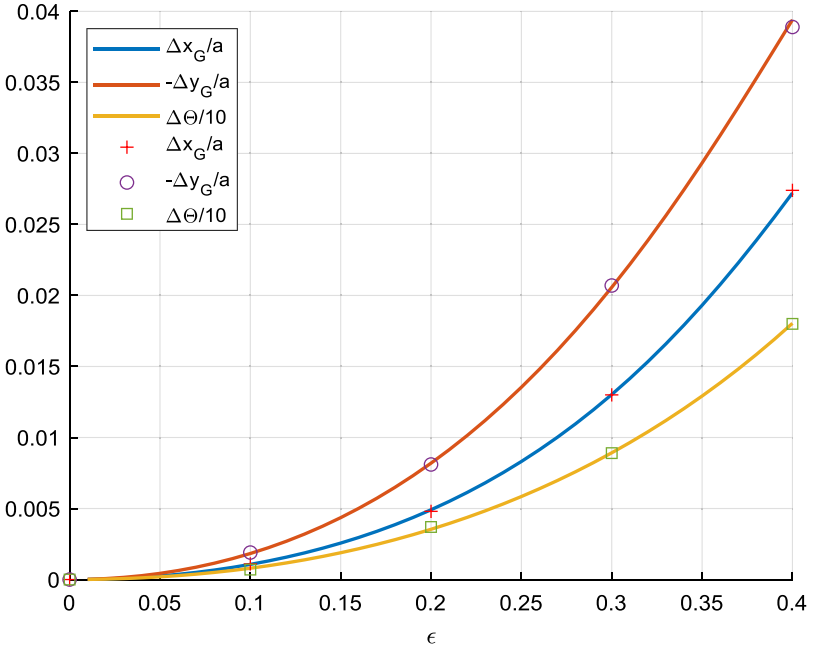

Figure 4. *Displacement and rotation for $L = 10a$ as a function of ϵ. The marks on the plot represent data obtained by Ebrahimian et al. in [25].*

a constant rate. In the next cycle, each arm, in turn, returns to its initial length with the same rate. In the end, the swimmer has returned to its initial configuration. The order of steps is presented in Fig. 3.

After these six steps, the predator experiences a net center of mass displacement along with a net rotation. The displacement and rotation after a full cycle have been presented in Fig. 4, as a function of ϵ.

To validate our dynamic model, results from Ebrahimian et al. have also been illustrated in Fig. 4, which demonstrates that the results that have been obtained and presented in this paper are completely coincident with results from [25]. In the proceeding sections, we will present control strategies for controlling the motion of the low-Reynolds predator.

https://doi.org/10.1017/S0263574721000953 Published online by Cambridge University Press

3. Predator Position and Heading Control

In this section, our aim is to determine the control inputs in a way that the microswimmer's position and orientation track the desired trajectories. Eq. (16) consists of three equations and six variables. The lengths of each arm are the variables used to control the predator's motion. Consequently, one control strategy can involve controlling three variables such as x_1, y_1, and θ, where these variables, respectively, are the first sphere x and y positions and the first arm orientation. In this case, the first sphere is essentially the predator and must be able to successfully hunt down the prey. These three variables are controlled to follow desired paths x_{1d}, y_{1d}, and θ_d using proportional control with feed forward terms. x_{1d} and y_{1d} are the prey's x and y positions:

$$\dot{x}_1 = \dot{x}_{1d} - k_{p1}\,(x_1 - x_{1d}) = c_1, \tag{17}$$

$$\dot{y}_1 = \dot{y}_{1d} - k_{p2}\,(y_1 - y_{1d}) = c_2, \tag{18}$$

$$\dot{\theta} = \dot{\theta}_d - k_{p3}\,(\theta - \theta_{\mathrm{d}}) = c_3. \tag{19}$$

As a result, $\dot{x}_1$, $\dot{y}_1$, and $\dot{\theta}$ are determined in each time step, and Eq. (16) can be merged with Eqs. (17) to (19) to produce the following system of equations:

$$\begin{bmatrix} 1 & 0 & 0 & 0 & 0 & 0 \\ 0 & 1 & 0 & 0 & 0 & 0 \\ 0 & 0 & 1 & 0 & 0 & 0 \\ \mathbf{M}_1\,(1,1) & \mathbf{M}_1\,(1,2) & \mathbf{M}_1\,(1,3) & \mathbf{M}_1\,(1,4) & \mathbf{M}_1\,(1,5) & \mathbf{M}_1\,(1,6) \\ \mathbf{M}_2\,(1,1) & \mathbf{M}_2\,(1,2) & \mathbf{M}_2\,(1,3) & \mathbf{M}_2\,(1,4) & \mathbf{M}_2\,(1,5) & \mathbf{M}_2\,(1,6) \\ \mathbf{M}_3\,(1,1) & \mathbf{M}_3\,(1,2) & \mathbf{M}_3\,(1,3) & \mathbf{M}_3\,(1,4) & \mathbf{M}_3\,(1,5) & \mathbf{M}_3\,(1,6) \end{bmatrix} \begin{bmatrix} \dot{x}_1 \\ \dot{y}_1 \\ \dot{\theta} \\ \dot{\mathrm{U}}_{12} \\ \dot{\mathrm{U}}_{23} \\ \dot{\mathrm{U}}_{31} \end{bmatrix} = \begin{bmatrix} c_1 \\ c_2 \\ c_3 \\ 0 \\ 0 \\ 0 \end{bmatrix}. \tag{20a}$$

Here, we have a system of six equations and six unknowns, which can be solved in each time step. Solving for $\dot{\mathrm{U}}_{12}$, $\dot{\mathrm{U}}_{23}$, and $\dot{\mathrm{U}}_{31}$ yields:

$$\boldsymbol{W} \begin{bmatrix} \dot{\mathrm{U}}_{12} \\ \dot{\mathrm{U}}_{23} \\ \dot{\mathrm{U}}_{31} \end{bmatrix} = \mathbf{Q} \begin{bmatrix} \dot{x}_{1d} - k_{p1}\,(x_1 - x_{1d}) \\ \dot{y}_{1d} - k_{p2}\,(y_1 - y_{1d}) \\ \dot{\theta}_d - k_{p3}\,(\theta - \theta_{\mathrm{d}}) \end{bmatrix} \tag{20b}$$

$$\boldsymbol{W} = \begin{bmatrix} \mathbf{M}_1\,(1,4) & \mathbf{M}_1\,(1,5) & \mathbf{M}_1\,(1,6) \\ \mathbf{M}_2\,(1,4) & \mathbf{M}_2\,(1,5) & \mathbf{M}_2\,(1,6) \\ \mathbf{M}_3\,(1,4) & \mathbf{M}_3\,(1,5) & \mathbf{M}_3\,(1,6) \end{bmatrix}, \quad \mathbf{Q} = -\begin{bmatrix} \mathbf{M}_1\,(1,1) & \mathbf{M}_1\,(1,2) & \mathbf{M}_1\,(1,3) \\ \mathbf{M}_2\,(1,1) & \mathbf{M}_2\,(1,2) & \mathbf{M}_2\,(1,3) \\ \mathbf{M}_3\,(1,1) & \mathbf{M}_3\,(1,2) & \mathbf{M}_3\,(1,3) \end{bmatrix}$$

The schematic of the employed control method and the details of controller block are shown in Fig. 5.

After variables $\dot{x}_1$, $\dot{y}_1$, $\dot{\theta}$, $\dot{\mathrm{U}}_{12}$, $\dot{\mathrm{U}}_{23}$, and $\dot{\mathrm{U}}_{31}$ are determined from, the velocity of each sphere (variables $\dot{x}_1$, $\dot{y}_1$, $\dot{x}_2$, $\dot{y}_2$, $\dot{x}_3$, and $\dot{y}_3$) can be determined using Eq. (13). Integrating the velocity of each sphere in each time step, results in the position vector of the next time step:

$$\begin{bmatrix} x_1 & y_1 & x_2 & y_2 & x_3 & y_3 \end{bmatrix}_{k+1} = \begin{bmatrix} x_1 & y_1 & x_2 & y_2 & x_3 & y_3 \end{bmatrix}_k + \Delta \mathrm{t} \begin{bmatrix} \dot{x}_1 & \dot{y}_1 & \dot{x}_2 & \dot{y}_2 & \dot{x}_3 & \dot{y}_3 \end{bmatrix}_k \tag{21}$$

For simulation, a time step of $\Delta \mathrm{t} = 0.01\mathrm{s}$ has been considered, which leads to convergent results over a simulation time span of 10 s. The following desired paths have been considered:

$$x_{1d} = (-2 - 0.6t)\ (\mu m)\,, \tag{22}$$

$$y_{1d} = \left(-3.75 - 5.85e^{-o.1t}\cos 0.7t\right)\ (\mu m)\,, \tag{23}$$

https://doi.org/10.1017/S0263574721000953 Published online by Cambridge University Press

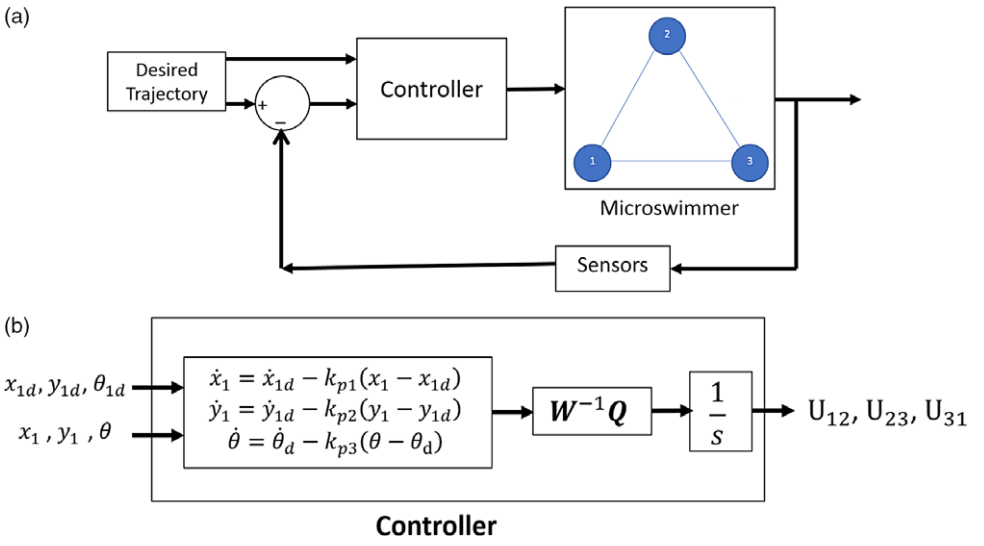

Figure 5. *Block diagram of the control system (a), controller block details (b).*

$$\theta_{\mathrm{d}} = \frac{\pi}{6}\,(rad)\,, \tag{24}$$

Control coefficients k_{p1} and k_{p2} are set equal to 1, k_{p3} is set at 0.5, initial values for x_1, y_1, and θ are assumed to be zero, and the initial arm lengths are 10 μm. The results are presented in the following figures.

Fig. 6 shows that the predator has been able to successfully hunt down its prey according to Eqs. (22), (23), and (24), and the position and angle errors have reduced to zero. The x and y positions have settled after almost 4 s, whereas the angle has taken almost 8 s to settle. This is due to the fact that the control coefficient for angle θ has been set at half that of x_1 and y_1. According to Eqs. (22), (23), and (24), the desired prey path for the predator lies on a curved line. This path, along with the predator's path, has been presented in Fig. 7, which shows their convergence.

The necessary arm length inputs have also been presented in Fig. 8. These results demonstrate that the arm length connecting spheres 1 and 3 has increased to almost 30 μm. While these results satisfy our control goals, it is desirable to decrease the amount and change of arm lengths in order to lower the swimmer's energy consumption. This can be achieved using optimal control strategies.

4. Optimal Control

An alternative control strategy is optimal control of the microswimmer position. Accordingly, variables x_1 and y_1, which are the predator's x and y positions, are controlled to follow reference paths $(x_1)_d$ and $(y_1)_d$, which are the prey's x and y positions, according to Eqs. (17) and (18), while minimizing an objective function J in each time step. Therefore, in each time step, variables θ_{k+1}, $U_{12_{k+1}}$, $U_{23_{k+1}}$, and $U_{31_{k+1}}$ must be determined such that they minimize function J while satisfying dynamical equations in relation (16). As a result, the Lagrange function to find minima of the objective function J, subject to the equality constraints (16), is the following:

$$\mathrm{L} = \mathrm{J} + (\gamma_1 \mathbf{M}_1 + \gamma_2 \mathbf{M}_2 + \gamma_3 \mathbf{M}_3)\,\dot{\mathbf{z}}. \tag{25}$$

https://doi.org/10.1017/S0263574721000953 Published online by Cambridge University Press

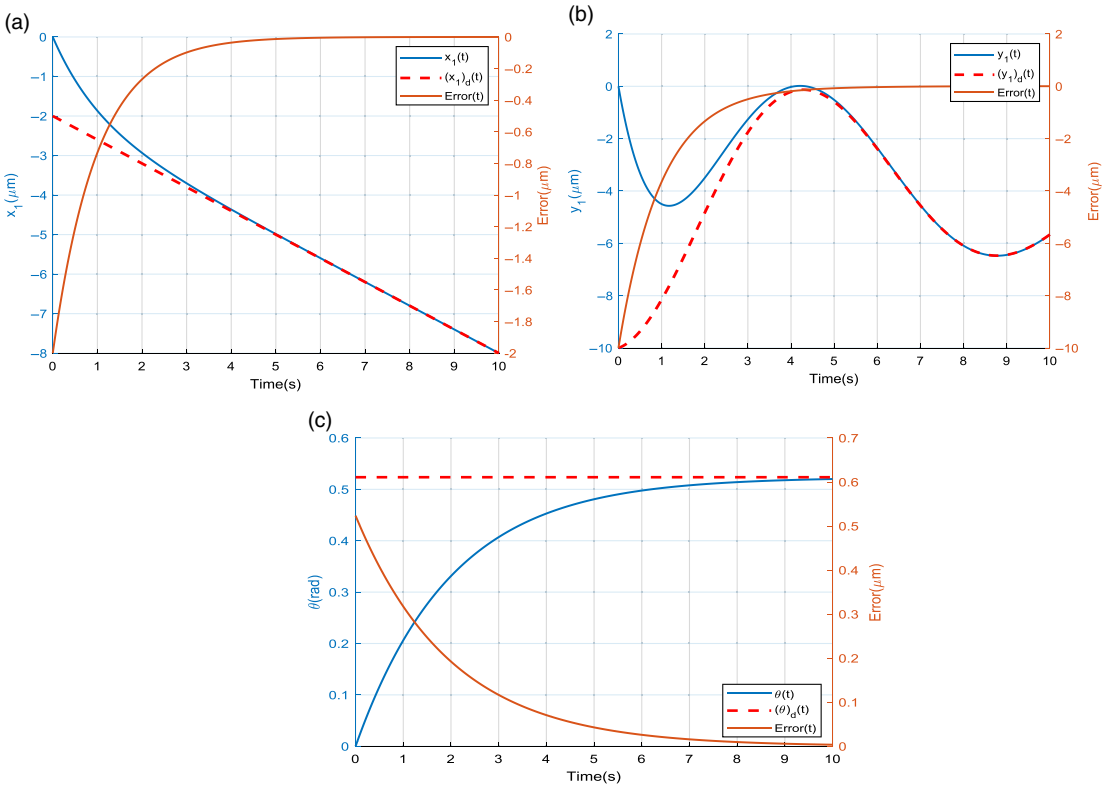

Figure 6. *(a) Position of x_1 and error as a function of time for control strategy involving control of position and angle. (b) Position of y_1 and error as a function of time for control strategy involving control of position and angle. (c) Angle θ and error as a function of time for control strategy involving control of position and angle.*

Here parameters γ_i are the Lagrange multipliers. The equations for optimal control in each time step are the following:

$$\begin{bmatrix}\mathbf{M}_1\\ \mathbf{M}_2\\ \mathbf{M}_3\end{bmatrix}\begin{bmatrix}\dot{x}_1\\ \dot{y}_1\\ \dot{\theta}\\ \dot{\mathrm{U}}_{12}\\ \dot{\mathrm{U}}_{23}\\ \dot{\mathrm{U}}_{31}\end{bmatrix}=\frac{\begin{bmatrix}\mathbf{M}_1\\ \mathbf{M}_2\\ \mathbf{M}_3\end{bmatrix}\left(\begin{bmatrix}x_1\\ y_1\\ \theta\\ \mathrm{U}_{12}\\ \mathrm{U}_{23}\\ \mathrm{U}_{31}\end{bmatrix}_{k+1}-\begin{bmatrix}x_1\\ y_1\\ \theta\\ \mathrm{U}_{12}\\ \mathrm{U}_{23}\\ \mathrm{U}_{31}\end{bmatrix}_{k}\right)}{\Delta \mathrm{t}}=0, \tag{26}$$

$$x_{1k+1}=x_{1k}+\Delta \mathrm{t}c_1,\quad y_{1k+1}=y_{1k}+\Delta \mathrm{t}c_2, \tag{27}$$

$$\frac{\partial \mathrm{L}}{\partial \theta_{k+1}}=\frac{\partial \mathrm{L}}{\partial \mathrm{U}_{12_{k+1}}}=\frac{\partial \mathrm{L}}{\partial \mathrm{U}_{23_{k+1}}}=\frac{\partial \mathrm{L}}{\partial \mathrm{U}_{31_{k+1}}}=0. \tag{28}$$

Relations (26) to (28) consist of 9 equations that are used to find $x_{1_{k+1}}, y_{1_{k+1}}, \theta_{k+1}, \mathrm{U}_{12_{k+1}}, \mathrm{U}_{23_{k+1}}, \mathrm{U}_{31_{k+1}}$, γ_1, γ_2, and γ_3. After that, positions of other spheres of the microswimmer can be found according to Eqs. (13) and (21).

https://doi.org/10.1017/S0263574721000953 Published online by Cambridge University Press

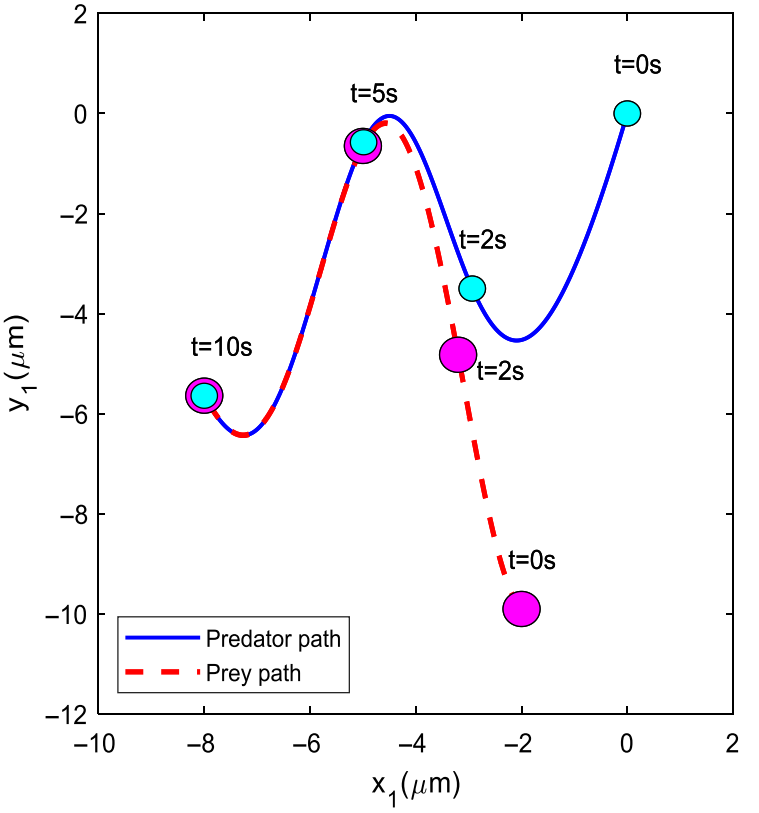

Figure 7. *The predator and prey paths for control strategy involving control of position and angle. The position of the first sphere (predator) and the prey at t=0, 2, 5, and 10 s has also been illustrated.*

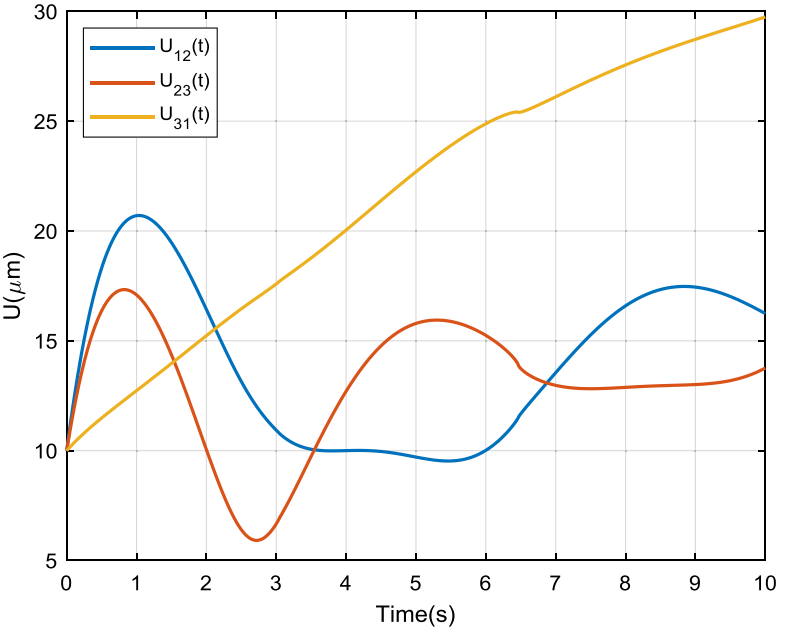

Figure 8. *Arm length between spheres as a function of time for control strategy involving control of position and angle.*

https://doi.org/10.1017/S0263574721000953 Published online by Cambridge University Press

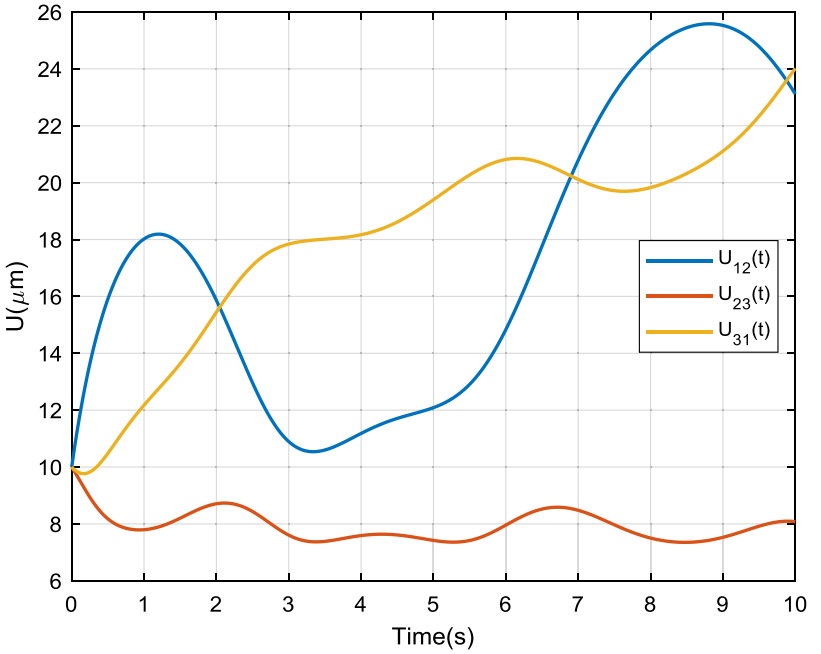

Figure 9. *Arm length between spheres as a function of time for optimal control strategy with objective function* J_1.

If the objective in each time step is to minimize fluctuations in the control efforts which are the swimmer arm lengths, the following objective function should be used:

$$J_1 = \frac{1}{2}\left[\left(U_{12_{k+1}} - U_{12_k}\right)^2 + \left(U_{23_{k+1}} - U_{23_k}\right)^2 + \left(U_{31_{k+1}} - U_{31_k}\right)^2\right]. \tag{29}$$

If it is desired to minimize arm lengths in the next time step, the following objective function is suitable:

$$J_2 = \frac{1}{2}\left[\left(U_{12_{k+1}} - b\right)^2 + \left(U_{23_{k+1}} - b\right)^2 + \left(U_{31_{k+1}} - b\right)^2\right]. \tag{30}$$

Reference arm length b should not be set too low; otherwise, the swimmer's arm lengths might decrease below 2 μm, resulting in collision between its spheres. Implementing J_2 results in undesirable shocks and impulses in the beginning of motion. In order to reduce the intensity of these shocks, a linear combination of J_1 and J_2 is used instead:

$$J_3 = J_1 + \alpha J_2 \tag{31}$$

The constant α shoud be small in order to avoid large impulses.

The swimmer's motion has been simulated for objective function J_1 and the following prey paths (22) and (23). Control coefficients k_{p1} and k_{p2} are set equal to 1, and initial values are similar to the previous simulation. The results are presented in the following figures:

The x and y positions of the first sphere are the same as the previous simulation in Fig. 6(a) and (b). Therefore, the predator has again been able to achieve the goal of tracking its prey, and both x and y positions of the first sphere (predator) have settled by $t = 4s$. In this case, however, the changes in arm lengths have decreased and the maximum arm length has been lowered by 5 μm, which can be seen in Fig. 9. The predator and prey paths for this simulation are the same as the previous simulation presented in Fig. 7.

The swimmer's motion has also been simulated for objective function J_3 and desired paths (22) and (23). Control coefficients k_{p1} and k_{p2} are set equal to 1, and initial conditions are the same as the previous

https://doi.org/10.1017/S0263574721000953 Published online by Cambridge University Press

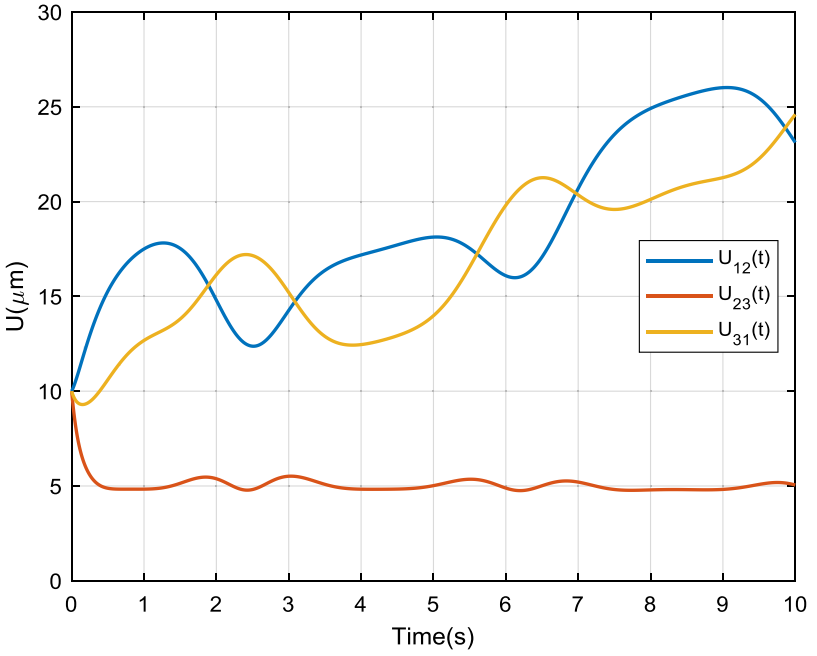

Figure 10. *Arm length between spheres as a function of time for optimal control strategy with objective function* J_3.

simulations. In Eq. (31), the constant α is set at 0.1, and reference arm length b is set at 7 μm. The results are presented in the following figure:

As before, the predator, which is the swimmer's first sphere, has been able to successfully hunt down the prey. The x and y positions of the first sphere are similar to previous simulations. Figure 10 illustrates the arm length inputs for the swimmer's motion. In this case, the arm length between spheres 2 and 3 has decreased quickly near to 5 μm, while peak arm length has only slightly increased compared to the previous simulation. The desired and actual paths for the predator and prey are similar to previous simulations.

5. Optimal Control with Constraints on the Arm Lengths

The optimal control strategies presented thus far do not place any constraints on the variations in arm lengths. In order to avoid spheres colliding with each other, or to limit the maximum increase of arm lengths, constraints must be considered for the minimum and maximum admissible values of the arm lengths. Controlling variables x_1 and y_1 to follow reference prey paths x_{1d} and y_{1d}, while minimizing objective function J with arm length constraints in each time step, is possible with quadratic programming. In order to use the quadratic programming technique, objective function J, system equations, and constraint inequalities can be written in matrix formulation [30]:

$$\min \frac{1}{2}\boldsymbol{x}^T\boldsymbol{H}\boldsymbol{x} + \boldsymbol{f}^T\boldsymbol{x}, \quad \text{S.t.}\boldsymbol{A}_{eq}\boldsymbol{x} = \boldsymbol{b}_{eq}, \quad \text{S.t.}\boldsymbol{lb} \le \boldsymbol{x} \le \boldsymbol{ub}. \tag{32}$$

In Eq. (32), $\boldsymbol{x}$ represents the vector containing variables that need to be determined. The term $\frac{1}{2}\boldsymbol{x}^T\boldsymbol{H}\boldsymbol{x} + \boldsymbol{f}^T\boldsymbol{x}$ is the quadratic objective or cost function which has been written in matrix formulation. The goal of quadratic programming is to minimize the objective function with constraints $\boldsymbol{A}_{eq}\boldsymbol{x} = \boldsymbol{b}_{eq}$ and $\boldsymbol{lb} \le \boldsymbol{x} \le \boldsymbol{ub}$. The term $\boldsymbol{A}_{eq}\boldsymbol{x} = \boldsymbol{b}_{eq}$ is the equality constraints of the system written in matrix formulation, and $\boldsymbol{lb}$ and $\boldsymbol{ub}$ are the lower and upper bounds of the variables.

https://doi.org/10.1017/S0263574721000953 Published online by Cambridge University Press

Here, we have presented the objective function for minimizing arm length change, J_1, in matrix form. J_1 can be expanded in the following form:

$$J_1 = \frac{1}{2}\left[{U_{12_{k+1}}}^2 + {U_{23_{k+1}}}^2 + {U_{31_{k+1}}}^2\right] - \left[U_{12_{k+1}}U_{12_k} + U_{23_{k+1}}U_{23_k} + U_{31_{k+1}}U_{31_k}\right]. \tag{33}$$

In Eq. (33), constant terms have been eliminated in the expansion of J_1. Therefore, $\boldsymbol{x}$, $\boldsymbol{H}$, and $\boldsymbol{f}$ are in the following order:

$$\boldsymbol{x} = \begin{bmatrix} x_1 \\ y_1 \\ \theta \\ U_{12} \\ U_{23} \\ U_{31} \end{bmatrix}_{k+1}, \quad \boldsymbol{H} = \begin{bmatrix} 0 & 0 & 0 & 0 & 0 & 0 \\ 0 & 0 & 0 & 0 & 0 & 0 \\ 0 & 0 & 0 & 0 & 0 & 0 \\ 0 & 0 & 0 & 1 & 0 & 0 \\ 0 & 0 & 0 & 0 & 1 & 0 \\ 0 & 0 & 0 & 0 & 0 & 1 \end{bmatrix}, \quad \boldsymbol{f} = \begin{bmatrix} 0 \\ 0 \\ 0 \\ -U_{12} \\ -U_{23} \\ -U_{31} \end{bmatrix}. \tag{34}$$

The dynamic equations for the system are Eqs. (16), (17), and (18), which if merged together, can be written in the following form:

$$\begin{bmatrix} 1 & 0 & 0 & 0 & 0 & 0 \\ 0 & 1 & 0 & 0 & 0 & 0 \\ \mathbf{M}_1(1,1) & \mathbf{M}_1(1,2) & \mathbf{M}_1(1,3) & \mathbf{M}_1(1,4) & \mathbf{M}_1(1,5) & \mathbf{M}_1(1,6) \\ \mathbf{M}_2(1,1) & \mathbf{M}_2(1,2) & \mathbf{M}_2(1,3) & \mathbf{M}_2(1,4) & \mathbf{M}_2(1,5) & \mathbf{M}_2(1,6) \\ \mathbf{M}_3(1,1) & \mathbf{M}_3(1,2) & \mathbf{M}_3(1,3) & \mathbf{M}_3(1,4) & \mathbf{M}_3(1,5) & \mathbf{M}_3(1,6) \end{bmatrix} \begin{bmatrix} \dot{x}_1 \\ \dot{y}_1 \\ \dot{\theta} \\ \dot{U}_{12} \\ \dot{U}_{23} \\ \dot{U}_{31} \end{bmatrix} = \begin{bmatrix} c_1 \\ c_2 \\ 0 \\ 0 \\ 0 \end{bmatrix} \tag{35}$$

Eq. (35) can be rewritten as the following expression:

$$\mathbf{R}\left[x_1 \;\; y_1 \;\; \theta \;\; U_{12} \;\; U_{23} \;\; U_{31}\right]_{k+1}^{\mathrm{T}} = \mathbf{R}\left[x_1 \;\; y_1 \;\; \theta \;\; U_{12} \;\; U_{23} \;\; U_{31}\right]_k^{\mathrm{T}} + \Delta t\left[c_1 \;\; c_2 \;\; 0 \;\; 0 \;\; 0\right]^{\mathrm{T}}, \tag{36}$$

where $\mathbf{R} = \begin{bmatrix} 1 & 0 & 0 & 0 & 0 & 0 \\ 0 & 1 & 0 & 0 & 0 & 0 \\ \mathbf{M}_1(1) & \mathbf{M}_1(2) & \mathbf{M}_1(3) & \mathbf{M}_1(4) & \mathbf{M}_1(5) & \mathbf{M}_1(6) \\ \mathbf{M}_2(1) & \mathbf{M}_2(2) & \mathbf{M}_2(3) & \mathbf{M}_2(4) & \mathbf{M}_2(5) & \mathbf{M}_2(6) \\ \mathbf{M}_3(1) & \mathbf{M}_3(2) & \mathbf{M}_3(3) & \mathbf{M}_3(4) & \mathbf{M}_3(5) & \mathbf{M}_3(6) \end{bmatrix}$. As a result, $\boldsymbol{A}_{eq}$ and $\boldsymbol{b}_{eq}$ are the following:

$$\boldsymbol{A}_{eq} = \mathbf{R}, \quad \boldsymbol{b}_{eq} = \mathbf{R}\left[x_1 \;\; y_1 \;\; \theta \;\; U_{12} \;\; U_{23} \;\; U_{31}\right]_k^{\mathrm{T}} + \Delta t\left[c_1 \;\; c_2 \;\; 0 \;\; 0 \;\; 0\right]^{\mathrm{T}}. \tag{37}$$

For simulation, the constraints for arm lengths are set between 8 and 25 μm. Therefore, the upper and lower bounds in (32) are the following:

$$\boldsymbol{lb} = \left[-\infty \;\; -\infty \;\; -\infty \;\; 8 \;\; 8 \;\; 8\right]^{\mathrm{T}}, \quad \boldsymbol{ub} = \left[+\infty \;\; +\infty \;\; +\infty \;\; 25 \;\; 25 \;\; 25\right]^{\mathrm{T}}. \tag{38}$$

After $x_{1_{k+1}}$, $y_{1_{k+1}}$, θ_{k+1}, $U_{12_{k+1}}$, $U_{23_{k+1}}$, and $U_{31_{k+1}}$ are determined in each time step from quadratic programming, the position vector of sphere centers, in the next time step, is determined using Eq. (13).

The swimmer's motion has been simulated for objective function J_1 and desired paths (22) and (23), with constraints according to (38). Control coefficients K_{p1} and K_{p2} are set equal to 1, and initial conditions are the same as the previous simulations. The results are presented in the Fig. 11. This figure presents arm length variations for this simulation. The results from Fig. 11 show that arm lengths have remained within their defined boundaries. However, as a result, overall arm length change has slightly increased, which, in turn, means more energy consumption. The predator and prey paths are similar to previous simulations.

The results from various proposed methods have been compared in Table I. According to this table, the last control strategy, optimal control with constraints on the arm lengths, not only minimizes the microswimmer length changes but also maintains the arms lengths in the desired interval.

https://doi.org/10.1017/S0263574721000953 Published online by Cambridge University Press

Table I. *The average of objective function J_1, average of objective function J_3 for the first second of motion, maximum arm length, minimum arm length, angle control ability, constraints on arm lengths, and settling time, for various simulations*

	Average J_1	**Average J_3 (from t = 0s to t = 1s)**	**Maximum arm length**	**Minimum arm length**	**Angle control**	**Constraint on arm lengths**
Position and Heading Control	0.0026 μm^2	10.7 μm^2	29.8 μm	5.9 μm	Yes	No
Objective Function J_1	0.0012 μm^2	4.6 μm^2	26.0 μm	7.4 μm	No	No
Objective Function J_3	0.0021 μm^2	4.2 μm^2	26.0 μm	4.8 μm	No	No
Length Constraints	0.0014 μm^2	4.6 μm^2	25.0 μm	8.0 μm	No	Yes

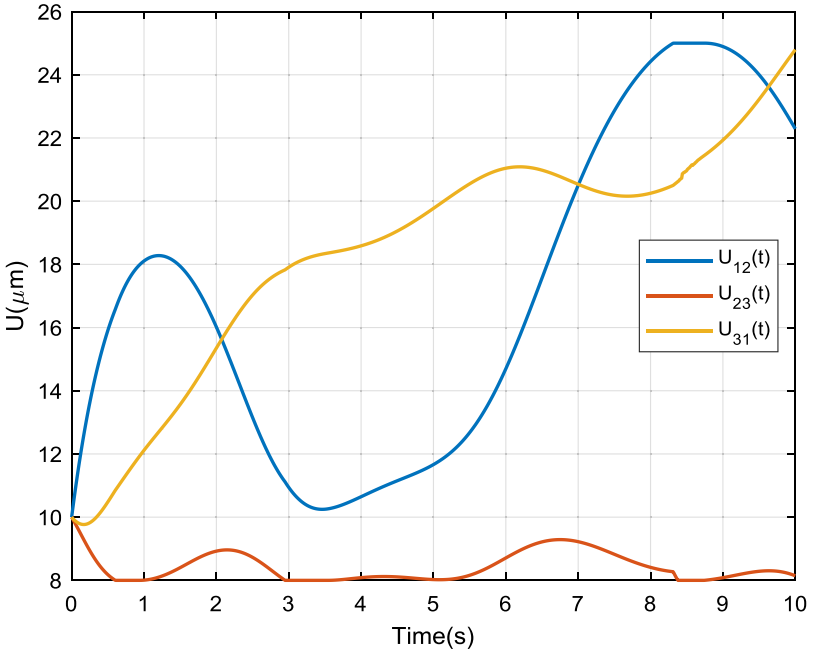

Figure 11. *Arm length between spheres as a function of time for optimal control strategy with objective function J_1 along with arm length constraints.*

6. Conclusion

In this paper, the dynamics and control of a triangular swimming microrobot were examined. Because of swimming at low Reynolds-number flow, the inertia forces are significantly smaller than viscous ones, and subsequently, Stokes equations are governed on the microrobot motion. After derivation of the dynamic equations governing on the motion, the position and orientation angle of the microswimmer were controlled to track desired time trajectories using proportional control with feed forward terms. The simulation results show that by changing its arm lengths, the robot was able to successfully track

https://doi.org/10.1017/S0263574721000953 Published online by Cambridge University Press

the desired trajectories. In order to reduce energy consumption and decrease arm length changes, optimal control was also proposed. In the end, optimal control of microswimmer, with constraints on arm lengths, was proposed. The results demonstrated that each arm length had remained within the permitted boundary and the desired trajectory had also been followed.

Acknowledgment. This work is financially supported by Iranian National Science Foundation (INSF).

Competing interests. The authors declare none.

References

[1] J. Gao, G. Yan, S. He, F. Xu and Z. Wang, "Design, analysis, and testing of a motor-driven capsule robot based on a sliding clamper," *Robotica*, **35**(3), 521–536 (2017).
[2] B. J. Nelson, I. K. Kaliakatsos and J. J. Abbott, "Microrobots for minimally invasive medicine," *Ann. Rev. Biomed. Eng.* **12**, 55–85 (2010).
[3] A. Kortschack, A. Shirinov, T. Trüper and S. Fatikow, "Development of mobile versatile nano handling microrobots: design, driving principles, haptic control," *Robotica*, **23**(4), 419–434 (2005).
[4] D. Ezzat, S. Amin, H. A. Shedeed and M. F. Tolba, "A new nano-robots control strategy for killing cancer cells using quorum sensing technique and directed particle swarm optimization algorithm," *Adv. Intell. Syst. Comput.* **921**, 218–226 (2020).
[5] D. Jang, J. Jeong, H. Song and S. K. Chung, "Targeted drug delivery technology using untethered microrobots: A review," *J. Micromechan. Microeng.* **29**(5), 053002 (2019).
[6] G. Ciuti, R. Caliò, D. Camboni, L. Neri, F. Bianchi, A. Arezzo, A. Koulaouzidis, S. Schostek, D. Stoyanov, C. M. Oddo, B. Magnani, A. Menciassi, M. Morino, M. O. Schurr and P. Dario, "Frontiers of robotic endoscopic capsules: A review," *J. Micro-Bio Robot.* **11**, 1–18 (2016).
[7] M. Medina-Sánchez, L. Schwarz, A. K. Meyer, F. Hebenstreit and O. G. Schmidt, "Cellular cargo delivery: Toward assisted fertilization by sperm-carrying micromotors," *Nano Lett.* **16**(1), 555–561 (2015).
[8] G. Cicconofri and A. DeSimone, "Modelling biological and bio-inspired swimming at microscopic scales: Recent results and perspectives," *Comput. Fluids*, **179**, 799–805 (2019).
[9] S. Palagi and P. Fischer, "Bioinspired microrobots," *Nat. Rev. Mater.* **3**, 113–124 (2018).
[10] H. Ning, Y. Zhang, H. Zhu, A. Ingham, G. Huang, Y. Mei and A. A. Solovev, "Geometry design, principles and assembly of micromotors," *Micromachines*, **9**(2), 75 (2018).
[11] S. Coyle, C. Majidi, P. LeDuc and K. J. Hsia, "Bio-inspired soft robotics: Material selection, actuation, and design," *Extr. Mech. Lett.* **22**, 51–59 (2018).
[12] D. Gong, J. Cai, N. Celi, L. Feng, Y. Jiang and D. Zhang, "Bio-inspired magnetic helical microswimmers made of nickel-plated Spirulina with enhanced propulsion velocity," *J. Magnet. Magnet. Mater.* **468**, 148–154 (2018).
[13] J. Liu, T. Xu, Y. Guan, X. Yan, C. Ye and X. Wu, "Swimming characteristics of bioinspired helical microswimmers based on soft lotus-root fibers," *Micromachines*, **8**(12), 349 (2017).
[14] H. Shum, "Microswimmer Propulsion by Two Steadily Rotating Helical Flagella," *Micromachines*, **10**(1), 65 (2019).
[15] E. Lushi, V. Kantsler and R. E. Goldstein, "Scattering of biflagellate microswimmers from surfaces," *Physical Review E*, **96**, 023102 (2017).
[16] H. Sayyaadi and S. Bahmanyar, "Development of a new mechanism to change velocity in a helical swimmer robot at low Reynolds number," *Sci. Iran.* **25**(5), 2616–2627 (2018).
[17] A. Nematollahisarvestani and A. Shamloo, "Dynamics of a magnetically rotated micro swimmer inspired by Paramecium metachronal wave," *Prog. Biophys. Mol. Biol.* **142**, 32–42 (2019).
[18] N. Sarvestani, A. Shamloo and M. T. Ahmadian, "Modeling paramecium swimming in a capillary tube," *Sci. Iran.* **23**(2), 658–667 (2016).
[19] I. S. M. Khalil, V. Magdanz, S. Sanchez, O. G. Schmidt and S. Misra, "Biocompatible, accurate, and fully autonomous: A sperm-driven micro-bio-robot," *J. Micro-Bio Robot.* **9**, 79–86 (2014).
[20] M. R. Edwards, R. W. Carlsen, J. Zhuang and M. Sitti, "Swimming characterization of Serratia marcescens for bio-hybrid micro-robotics," *J. Micro-Bio Robot.* **9**, 47–60 (2014).
[21] E. M. Purcell, "Life at low Reynolds number," *Am. J. Phys.* **45**, 3–11 (1977).
[22] B. Nasouri, A. Khot and G. J. Elfring, "Elastic two-sphere swimmer in Stokes flow," *Phys. Rev. Fluids*, **2**(4), 043101 (2017).
[23] C. Datt, B. Nasouri and G. J. Elfring, "Two-sphere swimmers in viscoelastic fluids," *Phys. Rev. Fluids*, **3**(12), 123301 (2018).
[24] M. S. Rizvi, A. Farutin and C. Misbah, "Three-bead steering microswimmers," *Phys. Rev. E*, **97**(2), 023102 (2018).
[25] M. Ebrahimian, M. Yekehzare and M. R. Ejtehadi, "Low-Reynolds-number predator," *Phys. Rev. E*, **92**, 063035 (2015).
[26] R. Khalesi, H. N. Pishkenari and G. Vossoughi, "Independent control of multiple magnetic microrobots: Design, dynamic modelling, and control," *J. Micro-Bio Robot.* **16**(2), 215–224, (2020).
[27] A. Esfandbod, H. N. Pishkenari and A. Meghdari, "Dynamics and control of a novel microrobot with high maneuverability," *Robotica*, 1–10 (2021).
[28] J. Happel and H. Brenner, "The Behavior of Fluids in Slow Motion," **In:** *Low Reynolds Number Hydrodynamics* (R. J. Moreau, ed.) (1st edn., Martinus Nijhoff Publishers, The Hague, The Netherlands, 1983), pp. 23–57.

https://doi.org/10.1017/S0263574721000953 Published online by Cambridge University Press

[29] G. P. Alexander, C. M. Pooley and J. M. Yeomans, "Hydrodynamics of linked sphere model swimmers," *J. Phys. Condens. Matt.* **21**(20), 204108 (2009).
[30] D. Tonon, M. S. Aronna and D. Kalise (eds.), *Optimal Control: Novel Directions and Applications* (Vol. **1**, Springer, 2017).

Cite this article: H. Nejat Pishkenari and M. Mohebalhojeh (2022). "Optimal motion control of three-sphere based low-Reynolds number swimming microrobot", Robotica **40**, 1257–1273. https://doi.org/10.1017/S0263574721000953